

CP violation in charged Higgs boson decays in the MSSM with complex parameters

Ekaterina Christova¹

*Institute of Nuclear Research and Nuclear Energy,
Tzarigradsko Chaussee 72, Sofia 1784, Bulgaria*

Helmut Eberl², **Walter Majerotto**³

*Institut für Hochenergiephysik der Österreichischen Akademie der Wissenschaften,
A-1050 Vienna, Austria*

Sabine Kraml⁴

Theory Division, CERN, CH-1211 Geneva 23, Switzerland

Abstract

Supersymmetric loop contributions can lead to different decay rates of $H^+ \rightarrow t\bar{b}$ and $H^- \rightarrow b\bar{t}$. We calculate the decay rate asymmetry $\delta^{CP} = [\Gamma(H^+ \rightarrow t\bar{b}) - \Gamma(H^- \rightarrow b\bar{t})] / [\Gamma(H^+ \rightarrow t\bar{b}) + \Gamma(H^- \rightarrow b\bar{t})]$ at next-to-leading order in the MSSM with complex parameters. We analyse the parameter dependence of δ^{CP} with emphasis on the phases of A_t and A_b . It turns out that the most important contribution comes from the loop with stop, sbottom, and gluino. If this contribution is present, δ^{CP} can go up to 10–15% for $\tan\beta \sim 10$, and to $\sim 5\%$ for large values of $\tan\beta$.

¹e-mail: echristo@inrne.bas.bg

²e-mail: helmut@hephy.oeaw.ac.at

³e-mail: majer@hephy.oeaw.ac.at

⁴e-mail: sabine.kraml@cern.ch

1 Introduction

Already for some time, it has been customary to look for CP-violating effects beyond the Standard Model (SM). All extensions of the SM contain possible new sources of CP violation through additional CP-violating phases. In particular, in the Minimal Supersymmetric Standard Model (MSSM), the Higgs mixing parameter μ in the superpotential, two of the soft SUSY-breaking Majorana gaugino masses M_i ($i = 1, 2, 3$), and the trilinear couplings A_f (corresponding to a fermion f) can have physical phases, which cannot be rotated away without introducing phases in other couplings [1]. From the point of view of baryogenesis, one might hope that these phases are large [2]. On the other hand, the experimental limits on electron and neutron electric dipole moments (EDMs) [3], $|d^e| \leq 2.15 \times 10^{-13}$ e/GeV, $|d^n| \leq 5.5 \times 10^{-12}$ e/GeV, place severe constraints on the phase of μ , $\phi_\mu < \mathcal{O}(10^{-2})$ [4], for a typical SUSY mass scale of the order of a few hundred GeV. A larger ϕ_μ imposes fine-tuned relationships between this phase and other SUSY parameters [5]. CP-violating effects that might arise from $A_{u,d}$ (where u, d are light quarks) are very much suppressed as they are proportional to $m_{u,d}$. On the other hand, the trilinear couplings of the third generation $A_{t,b,\tau}$ can lead to significant CP-violation effects, especially in top quark physics [6]. Phases of μ and $A_{t,b,\tau}$ also affect the Higgs sector in a relevant way. Although the Higgs potential of the MSSM is invariant under CP at tree level, at loop level CP is sizeably violated by complex couplings [7, 8]. As a consequence, the three neutral Higgs mass eigenstates are superpositions of the CP eigenstates h^0 , H^0 , and A^0 .

In this paper, we study CP violation in the decays $H^+ \rightarrow t\bar{b}$ and $H^- \rightarrow b\bar{t}$ in the MSSM with complex parameters. In particular, we calculate the CP-violating asymmetry

$$\delta^{CP} = \frac{\Gamma(H^+ \rightarrow t\bar{b}) - \Gamma(H^- \rightarrow b\bar{t})}{\Gamma(H^+ \rightarrow t\bar{b}) + \Gamma(H^- \rightarrow b\bar{t})}, \quad (1)$$

due to one-loop exchanges of \tilde{t} , \tilde{b} , \tilde{g} , $\tilde{\chi}^\pm$, $\tilde{\chi}^0$, and H^0 , see Fig. 1, taking into account CP violation in the neutral Higgs system according to [8]. Of course, the diagrams of Fig. 1 only contribute to δ^{CP} if they have an absorptive part. Since ϕ_μ is highly constrained, the most important phases in our analysis are ϕ_t and ϕ_b , the phases of A_t and A_b . Therefore, we expect the graph with \tilde{t} , \tilde{b} , and \tilde{g} in the loop to be the most important one, and δ^{CP} to be large in the case

$m_{H^+} > m_{\tilde{t}_1} + m_{\tilde{b}_1}$. In principle, there would also be a contribution due to $\tilde{\nu}$ and $\tilde{\tau}$ exchange analogous to Fig. 1e. However, this can be neglected in our study.

The paper is organized as follows: In Section 2 we give the basic formulae for the $H^\pm \rightarrow tb$ decays and define the decay rate asymmetry δ^{CP} at the 1-loop level in terms of CP-violating form factors δY_i^{CP} ($i = t, b$). The explicit expressions for $\delta Y_{t,b}^{CP}$ due to the diagrams of Fig. 1 are given in Section 3. In Section 4, we perform a detailed numerical analysis. In Section 5, we summarize our results and comment on the feasibility of measuring the CP-violating asymmetry δ^{CP} . Appendices A, B, and C contain the necessary mass and mixing matrices, the couplings, and the definition of the two- and three-point functions used in this paper.

2 The H^\pm decay

The matrix elements of the $H^+ \rightarrow t\bar{b}$ and $H^- \rightarrow b\bar{t}$ decays can be written as

$$\mathcal{M}_{H^+} = \bar{u}(p_t) [Y_b^+ P_R + Y_t^+ P_L] v(-p_b), \quad (2)$$

$$\mathcal{M}_{H^-} = \bar{u}(p_b) [Y_t^- P_R + Y_b^- P_L] v(-p_t), \quad (3)$$

with $P_{R,L} = \frac{1}{2}(1 \pm \gamma_5)$ and the loop-corrected couplings

$$Y_i^\pm = y_i + \delta Y_i^\pm \quad (i = t, b); \quad (4)$$

y_t and y_b are the tree-level couplings,

$$y_t = h_t \cos \beta, \quad y_b = h_b \sin \beta, \quad (5)$$

with h_t and h_b the top and bottom Yukawa couplings. The decay widths at tree level are given by

$$\Gamma^0(H^\pm \rightarrow tb) = \frac{3\kappa}{16\pi m_{H^\pm}^3} [(m_{H^\pm}^2 - m_t^2 - m_b^2)(y_t^2 + y_b^2) - 4m_t m_b y_t y_b], \quad (6)$$

where $\kappa = \kappa(m_{H^\pm}^2, m_t^2, m_b^2)$, $\kappa(x, y, z) = [(x - y - z)^2 - 4yz]^{1/2}$. Since there is no CP violation at tree level, $\Gamma^0(H^+ \rightarrow t\bar{b}) \equiv \Gamma^0(H^- \rightarrow b\bar{t})$. At next-to-leading order (NLO) we have

$$\begin{aligned} \Gamma(H^\pm \rightarrow tb) = \frac{3\kappa}{16\pi m_{H^\pm}^3} & [(m_{H^\pm}^2 - m_t^2 - m_b^2)(y_t^2 + y_b^2 + 2y_t \operatorname{Re} \delta Y_t^\pm + 2y_b \operatorname{Re} \delta Y_b^\pm) \\ & - 4m_t m_b (y_t y_b + y_t \operatorname{Re} \delta Y_b^\pm + y_b \operatorname{Re} \delta Y_t^\pm)] . \end{aligned} \quad (7)$$

The form factors δY_i^\pm ($i = t, b$) have, in general, both CP-invariant and CP-violating contributions:

$$\delta Y_i^\pm = \delta Y_i^{inv} \pm \frac{1}{2} \delta Y_i^{CP}. \quad (8)$$

Both the CP-invariant and the CP-violating contributions have real and imaginary (absorptive) parts. CP invariance implies that the form factors of H^+ and H^- are equal. Using Eqs. (7) and (8), we can write the CP-violating asymmetry δ^{CP} of Eq. (1) as

$$\delta^{CP} = \frac{\Delta (y_t \text{Re} \delta Y_t^{CP} + y_b \text{Re} \delta Y_b^{CP}) - 2m_t m_b (y_t \text{Re} \delta Y_b^{CP} + y_b \text{Re} \delta Y_t^{CP})}{\Delta (y_t^2 + y_b^2) - 4m_t m_b y_t y_b}, \quad (9)$$

where $\Delta = m_{H^+}^2 - m_t^2 - m_b^2$.

At one loop, there are six generic diagrams that may contribute to δ^{CP} . These are (A) triangle diagrams with (i) two fermions and a scalar, (ii) two scalars and a fermion, and (iii) a scalar, a vector boson and a fermion in the loop, and (B) $H^+ - W^+$ self-energy diagrams with (i) two fermions, (ii) two scalars, and (iii) a scalar and a vector boson in the loop. In the following, we work out the formulae for δY_i^{CP} for the specific case of the MSSM with complex phases. The relevant Feynman diagrams are shown in Fig. 1.

3 CP-violating contributions

3.1 Generic diagrams

According to Eqs. (2) and (4) we write the matrix elements of the 1-loop diagrams of Fig. 1 as

$$\mathcal{M}_{H^+} = \bar{u}(p_t) [\delta Y_b^+ P_R + \delta Y_t^+ P_L] v(-p_b), \quad (10)$$

and analogously for the H^- decay. In fact, we are only interested in the CP-violating parts $\text{Re} \delta Y_i^{CP}$. Since $\text{Re} \delta Y_i^{CP} = \text{Re} (\delta Y_i^+ - \delta Y_i^-)$, we just need the structure $\text{Im}(g_0 g_1 g_2) \times \text{Im}(PaVe)$ of the form factors δY_b^+ and δY_t^+ . Here $g_0 g_1 g_2$ stands for the product of the couplings and $PaVe$ for the Passarino–Veltman two- and three-point functions [9] B_0 and $C_{0,1,2}$. In the following, we give the formulae for the various contributions to $\text{Re} \delta Y_{t,b}^{CP}$. The necessary MSSM mass and

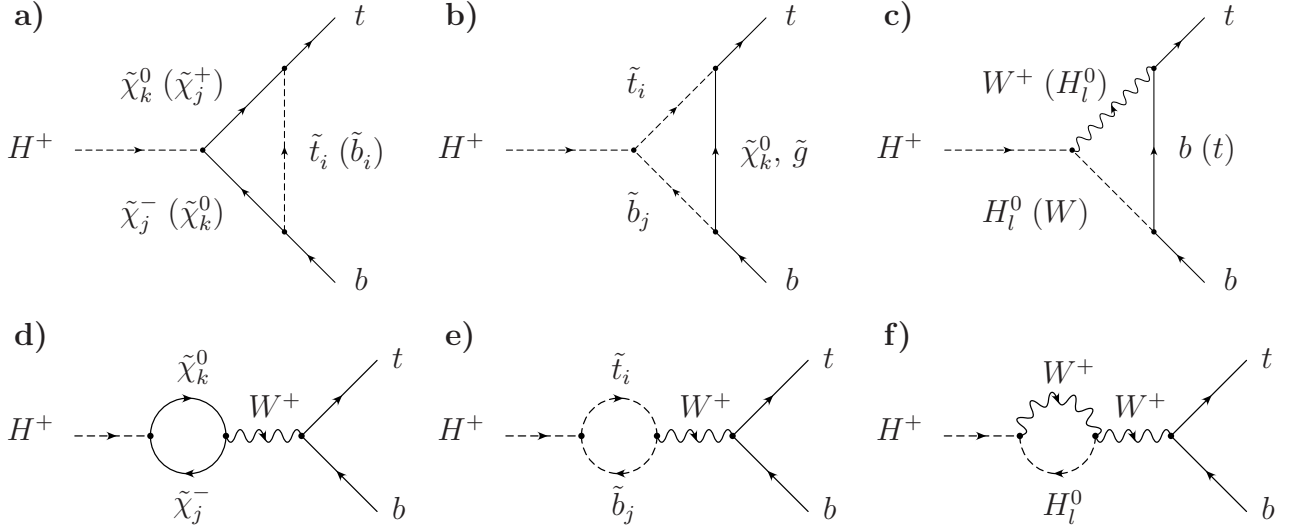


Figure 1: Sources for CP violation in $H^+ \rightarrow t\bar{b}$ decays at 1-loop level in the MSSM with complex couplings ($i, j = 1, 2$; $k = 1, \dots, 4$; $l = 1, 2, 3$).

mixing matrices, the couplings, as well as the definition of the two- and three-point functions are given in Appendices A, B, and C.

3.2 Vertex graphs

3.2.1 Neutralino-chargino-stop (sbottom) loop

The graph of Fig. 1a, with a neutralino, a chargino, and a stop in the loop, leads to

$$\begin{aligned}
 \text{Re } \delta Y_b^{CP}(\tilde{\chi}_k^0 \tilde{\chi}_j^\pm \tilde{t}_i) = \frac{1}{8\pi^2} \Big\{ & \left[m_t m_b \text{Im}(F_{jk}^R b_{ik}^{\tilde{t}} l_{ij}^{\tilde{t}*}) + m_{\tilde{\chi}_j^+} m_{\tilde{\chi}_k^0} \text{Im}(F_{jk}^R a_{ik}^{\tilde{t}} k_{ij}^{\tilde{t}*}) + m_t m_{\tilde{\chi}_j^+} \text{Im}(F_{jk}^R b_{ik}^{\tilde{t}} k_{ij}^{\tilde{t}*}) \right. \\
 & \left. + m_b m_{\tilde{\chi}_k^0} \text{Im}(F_{jk}^R a_{ik}^{\tilde{t}} l_{ij}^{\tilde{t}*}) + m_{\tilde{t}_i}^2 \text{Im}(F_{jk}^L a_{ik}^{\tilde{t}} k_{ij}^{\tilde{t}*}) \right] \text{Im}(C_0) \\
 & + m_t \left[m_t \text{Im}(F_{jk}^L a_{ik}^{\tilde{t}} k_{ij}^{\tilde{t}*}) + m_{\tilde{\chi}_k^0} \text{Im}(F_{jk}^L b_{ik}^{\tilde{t}} k_{ij}^{\tilde{t}*}) + m_b \text{Im}(F_{jk}^R b_{ik}^{\tilde{t}} l_{ij}^{\tilde{t}*}) + m_{\tilde{\chi}_j^+} \text{Im}(F_{jk}^R b_{ik}^{\tilde{t}} k_{ij}^{\tilde{t}*}) \right] \text{Im}(C_1) \\
 & + m_b \left[m_t \text{Im}(F_{jk}^R b_{ik}^{\tilde{t}} l_{ij}^{\tilde{t}*}) + m_{\tilde{\chi}_k^0} \text{Im}(F_{jk}^R a_{ik}^{\tilde{t}} l_{ij}^{\tilde{t}*}) + m_b \text{Im}(F_{jk}^L a_{ik}^{\tilde{t}} k_{ij}^{\tilde{t}*}) + m_{\tilde{\chi}_j^+} \text{Im}(F_{jk}^L a_{ik}^{\tilde{t}} l_{ij}^{\tilde{t}*}) \right] \text{Im}(C_2) \\
 & \left. + \text{Im}(F_{jk}^L a_{ik}^{\tilde{t}} k_{ij}^{\tilde{t}*}) \text{Im}(B_0(m_{H^+}^2, m_{\tilde{\chi}_k^0}^2, m_{\tilde{\chi}_j^+}^2)) \right\}, \tag{11}
 \end{aligned}$$

with $C_X = C_X(m_t^2, m_{H^+}^2, m_b^2, m_{\tilde{t}_i}^2, m_{\tilde{\chi}_k^0}^2, m_{\tilde{\chi}_j^+}^2)$, $X = 0, 1, 2$, the three-point functions [9] in the notation of [10]; $\text{Re } \delta Y_t^{CP}(\tilde{\chi}_k^0 \tilde{\chi}_j^\pm \tilde{t}_i)$ is obtained from Eq. (11) by interchanging $F_{jk}^{L \leftrightarrow R}$, $a_{ik}^{\tilde{t}} \leftrightarrow b_{ik}^{\tilde{t}}$,

$$k_{ij}^{\tilde{t}*} \leftrightarrow l_{ij}^{\tilde{t}*}.$$

The contribution from the neutralino–chargino–sbottom loop has exactly the same structure. Therefore, $\text{Re } \delta Y_b^{CP}(\tilde{\chi}_k^0 \tilde{\chi}_j^\pm \tilde{b}_i)$ is obtained from Eq. (11) by the following substitutions: for the masses of the loop particles $m_{\tilde{\chi}_k^0} \rightarrow m_{\tilde{\chi}_j^+}$, $m_{\tilde{\chi}_j^+} \rightarrow m_{\tilde{\chi}_k^0}$, $m_{\tilde{t}_i} \rightarrow m_{\tilde{b}_i}$; for the couplings $a_{ik}^{\tilde{t}} \rightarrow l_{ij}^{\tilde{b}}$, $b_{ik}^{\tilde{t}} \rightarrow k_{ij}^{\tilde{b}}$, $k_{ij}^{\tilde{t}*} \rightarrow b_{ik}^{\tilde{b}*}$, and $l_{ij}^{\tilde{t}*} \rightarrow a_{ik}^{\tilde{b}*}$; and analogously for $\text{Re } \delta Y_t^{CP}(\tilde{\chi}_k^0 \tilde{\chi}_j^\pm \tilde{b}_i)$.

3.2.2 Stop–sbottom–neutralino loop

The stop–sbottom–neutralino loop of Fig. 1b gives

$$\begin{aligned} \text{Re } \delta Y_b^{CP}(\tilde{t}_i \tilde{b}_j \tilde{\chi}_k^0) &= \frac{1}{8\pi^2} \left[m_{\tilde{\chi}_k^0} \text{Im}(G_{4ij} a_{ik}^{\tilde{t}} b_{jk}^{\tilde{b}*}) \text{Im}(C_0) \right. \\ &\quad \left. - m_t \text{Im}(G_{4ij} b_{ik}^{\tilde{t}} b_{jk}^{\tilde{b}*}) \text{Im}(C_1) - m_b \text{Im}(G_{4ij} a_{ik}^{\tilde{t}} a_{jk}^{\tilde{b}*}) \text{Im}(C_2) \right], \quad (12) \end{aligned}$$

$$\begin{aligned} \text{Re } \delta Y_t^{CP}(\tilde{t}_i \tilde{b}_j \tilde{\chi}_k^0) &= \frac{1}{8\pi^2} \left[m_{\tilde{\chi}_k^0} \text{Im}(G_{4ij} b_{ik}^{\tilde{t}} a_{jk}^{\tilde{b}*}) \text{Im}(C_0) \right. \\ &\quad \left. - m_t \text{Im}(G_{4ij} a_{ik}^{\tilde{t}} a_{jk}^{\tilde{b}*}) \text{Im}(C_1) - m_b \text{Im}(G_{4ij} b_{ik}^{\tilde{t}} b_{jk}^{\tilde{b}*}) \text{Im}(C_2) \right], \quad (13) \end{aligned}$$

with $C_X = C_X(m_t^2, m_{H^+}^2, m_b^2, m_{\tilde{\chi}_k^0}^2, m_{\tilde{t}_i}^2, m_{\tilde{b}_j}^2)$.

3.2.3 Stop–sbottom–gluino loop

The contribution from the diagram with a stop, a sbottom, and a gluino in Fig. 1b is

$$\begin{aligned} \text{Re } \delta Y_b^{CP}(\tilde{t}_i \tilde{b}_j \tilde{g}) &= -\frac{4}{3} \frac{\alpha_s}{\pi} \left[m_{\tilde{g}} \text{Im}(G_{4ij} R_{1i}^{\tilde{t}*} R_{2j}^{\tilde{b}} e^{i\phi_3}) \text{Im}(C_0) \right. \\ &\quad \left. + m_t \text{Im}(G_{4ij} R_{2i}^{\tilde{t}*} R_{2j}^{\tilde{b}}) \text{Im}(C_1) + m_b \text{Im}(G_{4ij} R_{1i}^{\tilde{t}*} R_{1j}^{\tilde{b}}) \text{Im}(C_2) \right], \quad (14) \end{aligned}$$

$$\begin{aligned} \text{Re } \delta Y_t^{CP}(\tilde{t}_i \tilde{b}_j \tilde{g}) &= -\frac{4}{3} \frac{\alpha_s}{\pi} \left[m_{\tilde{g}} \text{Im}(G_{4ij} R_{2i}^{\tilde{t}*} R_{1j}^{\tilde{b}} e^{-i\phi_3}) \text{Im}(C_0) \right. \\ &\quad \left. + m_t \text{Im}(G_{4ij} R_{1i}^{\tilde{t}*} R_{1j}^{\tilde{b}}) \text{Im}(C_1) + m_b \text{Im}(G_{4ij} R_{2i}^{\tilde{t}*} R_{2j}^{\tilde{b}}) \text{Im}(C_2) \right], \quad (15) \end{aligned}$$

with $C_X = C_X(m_t^2, m_{H^+}^2, m_b^2, m_{\tilde{g}}^2, m_{\tilde{t}_i}^2, m_{\tilde{b}_j}^2)$ and $\alpha_s = g_s^2/(4\pi)$.

3.2.4 W boson–neutral Higgs–bottom (top) loop

There are two contributions, one with a bottom and one with a top quark in the loop (with H_l^0 and W interchanged), see Fig. 1c. We use the $\xi = 1$ gauge. The $WH_l b$ loop gives:

$$\begin{aligned} \text{Re } \delta Y_b^{CP}(WH_l b) = & - \frac{\sqrt{2} g^2}{32\pi^2} \left\{ \text{Im}(X_b^R) [(3m_b^2 - 2m_{H_l}^2) \text{Im}(C_0) + m_t^2 \text{Im}(C_1) + 2m_b^2 \text{Im}(C_2)] \right. \\ & + \text{Im}(B_0(m_{H^+}^2, m_W^2, m_{H_l}^2)) - 2 \text{Im}(B_0(m_t^2, m_b^2, m_W^2)) \\ & \left. + m_b^2 \text{Im}(X_b^L) \text{Im}(2C_0 + C_2) \right\}, \end{aligned} \quad (16)$$

$$\text{Re } \delta Y_t^{CP}(WH_l b) = - \frac{\sqrt{2} g^2}{32\pi^2} m_t m_b [\text{Im}(X_b^R) \text{Im}(2C_1 + C_2) + \text{Im}(X_b^L) \text{Im}(C_1 - C_0)], \quad (17)$$

where $X_b^R = g_{H_l H^+ W^-} s_l^{b,R}$, $X_b^L = g_{H_l H^+ W^-} s_l^{b,L}$, and $C_X = C_X(m_t^2, m_{H^+}^2, m_b^2, m_b^2, m_W^2, m_{H_l}^2)$. Analogously, the $H_l W t$ loop gives

$$\begin{aligned} \text{Re } \delta Y_b^{CP}(H_l W t) = & \frac{\sqrt{2} g^2}{32\pi^2} m_t m_b [\text{Im}(X_t^L) \text{Im}(2C_1 + C_2) + \text{Im}(X_t^R) \text{Im}(C_1 - C_0)], \quad (18) \\ \text{Re } \delta Y_t^{CP}(H_l W t) = & \frac{\sqrt{2} g^2}{32\pi^2} \left\{ \text{Im}(X_t^L) [(3m_t^2 - 2m_{H_l}^2) \text{Im}(C_0) + m_b^2 \text{Im}(C_1) + 2m_t^2 \text{Im}(C_2)] \right. \\ & + \text{Im}(B_0(m_{H^+}^2, m_W^2, m_{H_l}^2)) - 2 \text{Im}(B_0(m_b^2, m_t^2, m_W^2)) \\ & \left. + m_t^2 \text{Im}(X_t^R) \text{Im}(2C_0 + C_2) \right\}, \end{aligned} \quad (19)$$

with $X_t^R = g_{H_l H^+ W^-} s_l^{t,R}$, $X_t^L = g_{H_l H^+ W^-} s_l^{t,L}$, and $C_X = C_X(m_t^2, m_{H^+}^2, m_b^2, m_t^2, m_{H_l}^2, m_W^2)$.

3.2.5 Ghost–neutral Higgs–bottom (top) loop

Since the above graphs with a W boson are calculated in the $\xi = 1$ gauge, we also have to include the corresponding graphs with $W^\pm \rightarrow G^\pm$. These lead to

$$\begin{aligned} \text{Re } \delta Y_b^{CP}(GH_l b) = & - \frac{1}{8\pi^2} \left[m_b h_b \cos \beta \text{Im}(\hat{X}_b^R) \text{Im}(C_0) + m_t h_t \sin \beta \text{Im}(\hat{X}_b^R) \text{Im}(C_1) \right. \\ & \left. - m_b h_b \cos \beta \text{Im}(\hat{X}_b^L) \text{Im}(C_2) \right], \end{aligned} \quad (20)$$

$$\begin{aligned} \text{Re } \delta Y_t^{CP}(GH_l b) = & \frac{1}{8\pi^2} \left[m_b h_t \sin \beta \text{Im}(\hat{X}_b^L) \text{Im}(C_0) + m_t h_b \cos \beta \text{Im}(\hat{X}_b^L) \text{Im}(C_1) \right. \\ & \left. - m_b h_t \sin \beta \text{Im}(\hat{X}_b^R) \text{Im}(C_2) \right], \end{aligned} \quad (21)$$

and

$$\begin{aligned} \text{Re } \delta Y_b^{CP}(H_l G t) = & -\frac{1}{8\pi^2} \left[m_t h_b \cos \beta \text{Im}(\hat{X}_t^R) \text{Im}(C_0) - m_t h_b \cos \beta \text{Im}(\hat{X}_t^L) \text{Im}(C_1) \right. \\ & \left. + m_b h_t \sin \beta \text{Im}(\hat{X}_t^R) \text{Im}(C_2) \right], \end{aligned} \quad (22)$$

$$\begin{aligned} \text{Re } \delta Y_t^{CP}(H_l G t) = & \frac{1}{8\pi^2} \left[m_t h_t \sin \beta \text{Im}(\hat{X}_t^L) \text{Im}(C_0) - m_t h_t \sin \beta \text{Im}(\hat{X}_t^R) \text{Im}(C_1) \right. \\ & \left. + m_b h_b \cos \beta \text{Im}(\hat{X}_t^L) \text{Im}(C_2) \right]. \end{aligned} \quad (23)$$

Here, $\hat{X}_q^{R,L} = g_{H_l H^+ G^-} s_l^{qR,L}$ for $q = b, t$. The C functions are $C_X = C_X(m_t^2, m_{H^+}^2, m_b^2, m_b^2, m_W^2, m_{H_l}^2)$ for $q = b$ and $C_X = C_X(m_t^2, m_{H^+}^2, m_b^2, m_t^2, m_{H_l}^2, m_W^2)$ for $q = t$.

3.3 Self-energy graphs

3.3.1 Neutralino–chargino loop

The self-energy graph with a neutralino and a chargino of Fig. 1d gives

$$\begin{aligned} \text{Re } \delta Y_{b(t)}^{CP}(\tilde{\chi}_k^0 \tilde{\chi}_j^\pm - W) = & \pm \frac{1}{8\pi^2} \frac{g^2 m_{b(t)}}{\sqrt{2} m_{H^+}^2 m_W^2} \text{Im} \left(B_0(m_{H^+}^2, m_{\tilde{\chi}_k^0}^2, m_{\tilde{\chi}_j^\pm}^2) \right) \times \\ & \left[\text{Im}(c_{II}) m_{\tilde{\chi}_j^\pm} (m_{H^+}^2 + m_{\tilde{\chi}_k^0}^2 - m_{\tilde{\chi}_j^\pm}^2) - \text{Im}(c_{IJ}) m_{\tilde{\chi}_k^0} (m_{H^+}^2 - m_{\tilde{\chi}_k^0}^2 + m_{\tilde{\chi}_j^\pm}^2) \right] \end{aligned} \quad (24)$$

with $c_{II} = F_{jk}^R O_{kj}^R + F_{jk}^L O_{kj}^L$, and $c_{IJ} = F_{jk}^R O_{kj}^L + F_{jk}^L O_{kj}^R$. The overall plus sign is for δY_b^{CP} , and the overall minus sign for δY_t^{CP} .

3.3.2 Stop–sbottom loop

The graph of Fig. 1e leads to

$$\begin{aligned} \text{Re } \delta Y_{b(t)}^{CP}(\tilde{t}_i \tilde{b}_j - W) = & \mp \frac{3g^2}{16\pi^2} \frac{m_{b(t)}}{m_{H^+}^2 m_W^2} (m_{\tilde{t}_i}^2 - m_{\tilde{b}_j}^2) \times \\ & \text{Im}(G_{4ij} R_{1i}^{\tilde{t}} R_{1j}^{\tilde{b}*}) \text{Im} \left(B_0(m_{H^+}^2, m_{\tilde{b}_j}^2, m_{\tilde{t}_i}^2) \right). \end{aligned} \quad (25)$$

3.3.3 W^\pm – H_l^0 and G^\pm – H_l^0 loops

The self-energy graph with W^+ and H_l^0 is shown in Fig. 1f. Since we use $\xi = 1$ gauge for the W in the loop, we have to add the corresponding graph with a ghost, i.e. $W^\pm \rightarrow G^\pm$ in the

loop. (The second W propagator can be calculated in the unitary gauge. Hence, no ghost is necessary in this case.) The two contributions together give:

$$\begin{aligned} \text{Re } \delta Y_{b(t)}^{CP} (WH_l^0 - W) = \mp \frac{1}{32\pi^2} \frac{g^3 m_{b(t)}}{\sqrt{2} m_{H^+}^2 m_W} (2m_W^2 - 2m_{H_l}^2 - 3m_{H^+}^2) \times \\ O_{3l} (\cos \beta O_{1l} + \sin \beta O_{2l}) \text{Im} (B_0(m_{H^+}^2, m_{H_l}^2, m_W^2)) . \end{aligned} \quad (26)$$

4 Numerical results

Let us now turn to the numerical analysis. In order not to vary too many parameters, we fix part of the parameter space at the electroweak scale by the choice ⁵

$$\begin{aligned} M_2 = 200 \text{ GeV}, \quad \mu = -350 \text{ GeV}, \quad M_{\tilde{U}} : M_{\tilde{Q}} : M_{\tilde{D}} = 0.85 : 1 : 1.05, \\ A_t = A_b = -500 \text{ GeV}. \end{aligned} \quad (27)$$

Moreover, we assume GUT relations for the gaugino mass parameters M_1, M_2, M_3 . In this case, the phases of the gaugino sector can be rotated away. Since ϕ_μ , the phase of μ , is highly constrained by the EDMs of electron and neutron, we take $\phi_\mu = 0$. The phases relevant to our study are thus ϕ_t and ϕ_b , the phases of A_t and A_b .

The choice in Eq. (27) together with $M_{\tilde{Q}} = 490 \text{ GeV}$ and $\tan \beta = 10$ gives a mass spectrum quite similar to the Snowmass point SPS1a [11]. Figure 2 shows δ^{CP} for this case as a function of m_{H^+} in the range $m_{H^+} = 200 - 1400 \text{ GeV}$ and various values of ϕ_t . The sparticle masses are given explicitly in Table 1.

For $m_{H^+} < m_{\tilde{t}_1} + m_{\tilde{b}_1}$, δ^{CP} is very small, $\mathcal{O}(10^{-3})$ or smaller. The contributions to δ^{CP} come from the diagrams of Figs. 1a, 1c, and 1f; the diagram of Fig. 1d only contributes if there is a non-zero phase in the chargino/neutralino sector. In the region $m_{H^+} = 200 - 800 \text{ GeV}$, one can distinguish the thresholds of $\tilde{\chi}_1^0 \tilde{\chi}_1^\pm$ at $m_{H^+} \simeq 290 \text{ GeV}$, $\tilde{\chi}_1^0 \tilde{\chi}_2^\pm$ at $m_{H^+} \simeq 470 \text{ GeV}$, $\tilde{\chi}_3^0 \tilde{\chi}_1^\pm$ at

⁵In the original version of the paper [13] there were two mistakes in the analytic expressions [14], which also affected the numerical analysis: for $\tan \beta = 10$ (40) the results for δ^{CP} in [13] are reduced to about 30% (50%). However, one can easily find scenarios where δ^{CP} goes up to 10–15%. In particular, for the parameters of Eq. (27), the resulting plots are very similar to the original ones.

$\tan \beta$	$m_{\tilde{\chi}_1^0}$	$m_{\tilde{\chi}_2^0}$	$m_{\tilde{\chi}_3^0}$	$m_{\tilde{\chi}_4^0}$	$m_{\tilde{\chi}_1^+}$	$m_{\tilde{\chi}_2^+}$
10	99	191	359	369	191	372
40	98	188	358	372	188	374

$M_{\tilde{Q}}$	$\tan \beta$	$m_{\tilde{t}_1}$	$m_{\tilde{t}_2}$	$m_{\tilde{b}_1}$	$m_{\tilde{b}_2}$
490	10	384 (377)	568 (573)	486	522
	40	379 (377)	571 (573)	435	566
350	10	226 (213)	465 (471)	340	382
	40	216 (212)	470 (472)	257	443

Table 1: Sparticle masses (in GeV) for parameter sets used in the numerical analysis for $\phi_t = 0$ ($\frac{\pi}{2}$).

$m_{H^+} \simeq 550$ GeV, $\tilde{\chi}_2^0 \tilde{\chi}_2^\pm$ and $\tilde{\chi}_4^0 \tilde{\chi}_1^\pm$ at $m_{H^+} \simeq 560$ GeV, and $\tilde{\chi}_{3,4}^0 \tilde{\chi}_2^\pm$ at $m_{H^+} \simeq 730$ –740 GeV. Below the $\tilde{\chi}_1^0 \tilde{\chi}_1^\pm$ threshold, δ^{CP} originates only from the graphs with W and a neutral Higgs boson of Figs. 1c and 1f. Here note that the graph with $WH_l^0 b$ of Fig. 1c always contributes, since $m_t > m_W + m_b$.

However, once the $H^+ \rightarrow \tilde{t} \tilde{b}$ channel is open, δ^{CP} can go up to several per cent. The thresholds of $H^+ \rightarrow \tilde{t}_1 \tilde{b}_1$ at $m_{H^+} \sim 860$ GeV, and of $H^+ \rightarrow \tilde{t}_2 \tilde{b}_2$ at $m_{H^+} \sim 1100$ GeV are clearly visible in Fig. 2. For $m_{H^+} = 1$ TeV, we obtain $\delta^{CP} \simeq -3\%$, -6% , and -8% for $\phi_t = \frac{\pi}{8}$, $\frac{\pi}{4}$, and $\frac{\pi}{2}$, respectively. The dominant contribution comes from the stop–sbottom–gluino loop of Fig. 1b. Also the stop–sbottom–neutralino loop of Fig. 1b and the stop–sbottom self-energy of Fig. 1e can give a relevant contribution and should thus be taken into account. The contribution of the graphs with $\tilde{\chi}^\pm \tilde{\chi}^0$ or $H^0 W$ (Fig. 1a,c,f) exchange can, however, be neglected in this case.

The relative importance of the various contributions is illustrated in Fig. 3, where we plot the form factors $\text{Re } \delta Y_b^{CP}$ and $\text{Re } \delta Y_t^{CP}$ as functions of m_{H^+} , for $\phi_t = \pi/2$ and the other parameters as in Fig. 2. To calculate the contributions with neutral Higgs bosons, we have used [8, 12]. This is sufficient for our purpose, since we are mainly interested in large CP-violating effects that occur for $m_{H^+} > m_{\tilde{t}_1} + m_{\tilde{b}_1}$ because of $\phi_{t,b}$. However, once precision measurements of H^\pm

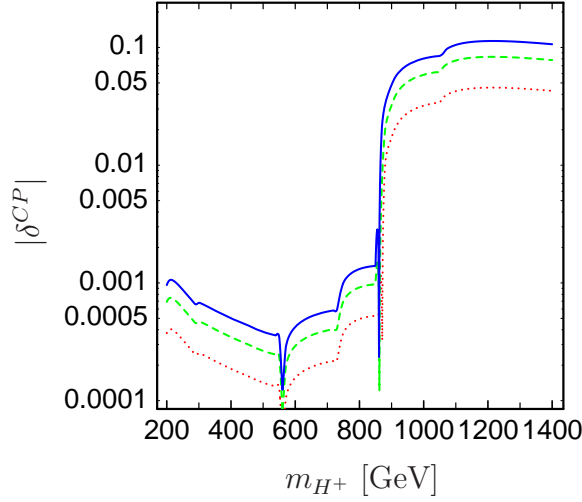


Figure 2: Absolute value of δ^{CP} as a function of m_{H^+} , for $M_{\tilde{Q}} = 490$ GeV and $\tan\beta = 10$. The solid, dashed, and dotted lines are for $\phi_t = \frac{\pi}{2}$, $\frac{\pi}{4}$, and $\frac{\pi}{8}$, respectively, $\phi_b = 0$, the other parameters are fixed by Eq. (27).

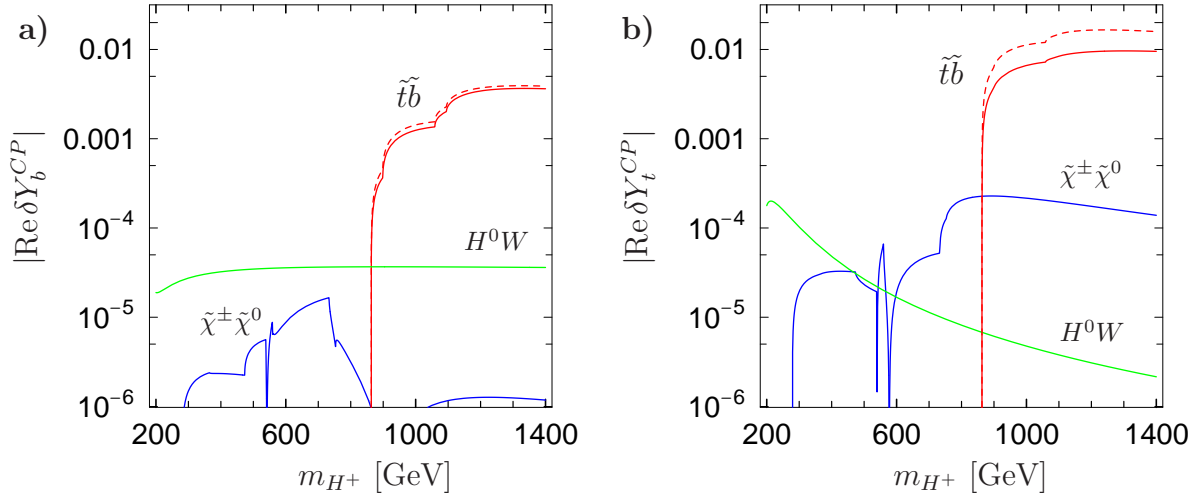


Figure 3: Absolute values of $\text{Re } \delta Y_b^{CP}$ and $\text{Re } \delta Y_t^{CP}$ as functions of m_{H^+} , for $\phi_t = \pi/2$ and the other parameters as in Fig. 2. The blue lines show the contribution from the $\tilde{\chi}^\pm \tilde{\chi}^0$ exchanges of Fig. 1a; the red lines are those from the $\tilde{t}\tilde{b}$ exchanges of Figs. 1b and 1e; the green lines are those from the diagrams with H^0 and W of Figs. 1c and 1f. The red dashed lines show $\text{Re } \delta Y_i^{CP}$ due to the $\tilde{t}\tilde{b}\tilde{g}$ loop only.

decays become feasible, a more complete calculation of the H_l^0 masses and couplings [15] might be used.

We next lower the stop/sbottom mass scale to $M_{\tilde{Q}} = 350$ GeV. The resulting masses are given in Table 1. Figures 4a and 4b show δ^{CP} for this case as functions of m_{H^+} and $\tan\beta$, respectively. The threshold behaviour of Fig. 4a is very similar to that of Fig. 2a. The threshold of $H^+ \rightarrow \tilde{t}_1 \tilde{b}_1$ is shifted to $m_{H^+} \simeq 550$ GeV, and δ^{CP} reaches larger values for lighter squarks. Even for a small phase ϕ_t , δ^{CP} can be a few per cent. Figure 4b shows the $\tan\beta$ dependence of δ^{CP} for $m_{H^+} = 700$ GeV and the cases $\phi_t = \pi/2$, $\phi_b = 0$ (full line) and $\phi_t = \phi_b = \pi/2$ (dashed line). For completeness, we also show as a dotted line the case of $\mu = +350$ GeV (with $\phi_t = \pi/2$, $\phi_b = 0$). It turns out that the asymmetry has a maximum around $\tan\beta \simeq 10$ and decreases for larger values of $\tan\beta$. In particular, we have $\delta^{CP} \sim -12\%$ (-3.5%) for $\tan\beta = 10$ (40), $\phi_t = \pi/2$, $\phi_b = 0$, and $\mu = -350$ GeV. An additional phase of A_b can enhance or reduce the asymmetry. For $\mu < 0$, however, its effects in the triangle and self-energy graphs of Fig. 1b and 1e compensate each other so that the overall dependence on ϕ_b is small. The dependence is larger for $\mu > 0$.

Here we also note that the branching ratio of $H^+ \rightarrow t\bar{b}$ increases with $\tan\beta$. In the case of vanishing phases we have $\text{BR}(H^+ \rightarrow t\bar{b}) \simeq 17\%$ (15%) at $\tan\beta = 10$ and 85% (75%) at $\tan\beta = 40$ for $M_{\tilde{Q}} = 350$ (490) GeV and $m_{H^+} = 700$ (1000) GeV.

The dependence on ϕ_t is shown explicitly in Fig. 5, where we plot δ^{CP} as a function of ϕ_t for $M_{\tilde{Q}} = 350$ GeV, $m_{H^+} = 700$ GeV, $\tan\beta = 10$ and 40 and various choices of ϕ_b . As expected, δ^{CP} shows a $\sim \sin\phi_t$ dependence.

Last but not least we relax the GUT relations between the gaugino masses and take $m_{\tilde{g}}$ as a free parameter (keeping, however, the relation between M_1 and M_2). Figure 6a shows the dependence of δ^{CP} on the gluino mass, for $M_{\tilde{Q}} = 350$ GeV, $m_{H^+} = 700$ GeV, $\phi_t = \pi/2$, and $\tan\beta = 10$ and 40 (keeping $M_3 = m_{\tilde{g}}$ real). It is interesting that there is still an effect for a large gluino mass: for $\tan\beta = 10$, δ^{CP} is reduced from about -12% to about -9% for $m_{\tilde{g}} = 600 \rightarrow 1200$ GeV. Also in the large $\tan\beta$ case, δ^{CP} is decreased by 30% when the gluino mass is doubled: from -3.4% to -2.4% for $m_{\tilde{g}} = 600 \rightarrow 1200$ GeV. A non-zero phase of M_3

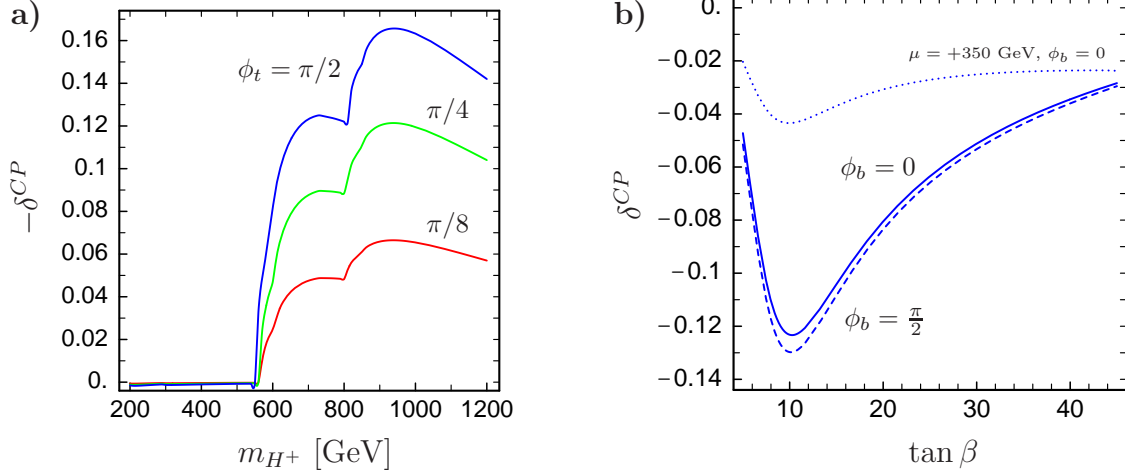


Figure 4: δ^{CP} for $M_{\tilde{Q}} = 350$ GeV; in (a) as a function of m_{H^+} , for $\tan \beta = 10$, $\phi_b = 0$, and in (b) as a function of $\tan \beta$, for $m_{H^+} = 700$ GeV and $\phi_t = \frac{\pi}{2}$. The other parameters are fixed by Eq. (27).

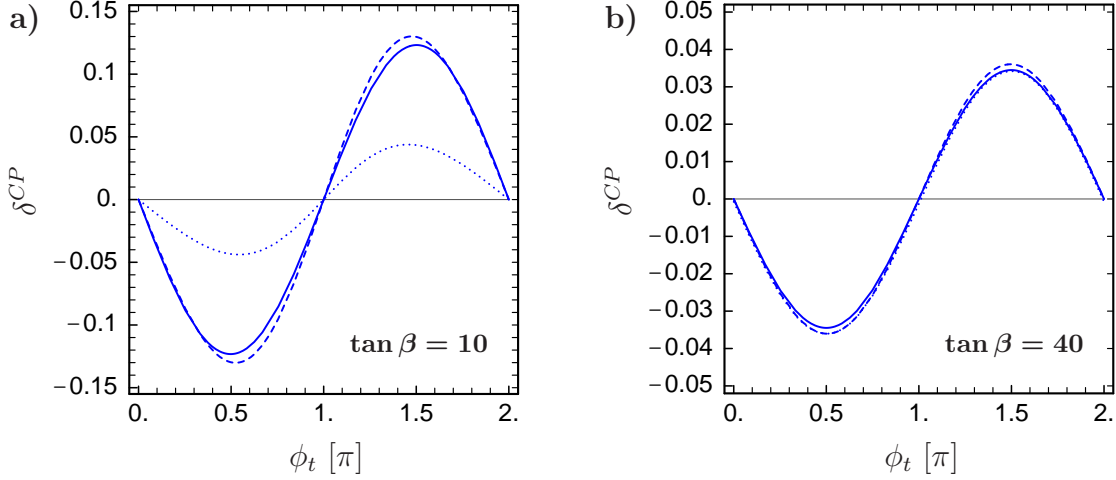


Figure 5: δ^{CP} as a function of ϕ_t , for $M_{\tilde{Q}} = 350$ GeV, $m_{H^+} = 700$ GeV, $\tan \beta = 10$ in (a) and $\tan \beta = 40$ in (b); full lines: $\phi_b = 0$, dashed lines: $\phi_b = \phi_t$, dotted lines: $\mu = 350$ GeV, $\phi_b = 0$. The other parameters are fixed by Eq. (27).

may also have a large effect. This is shown in Fig. 6b, where we plot δ^{CP} as a function of ϕ_3 for $m_{\tilde{g}} = |M_3| = 565$ GeV and $\phi_t = 0$ and $\pi/2$. In both cases, the asymmetry can be $\mathcal{O}(10\%)$. For $\mu > 0$, the curves are shifted but the order of magnitude does not change.

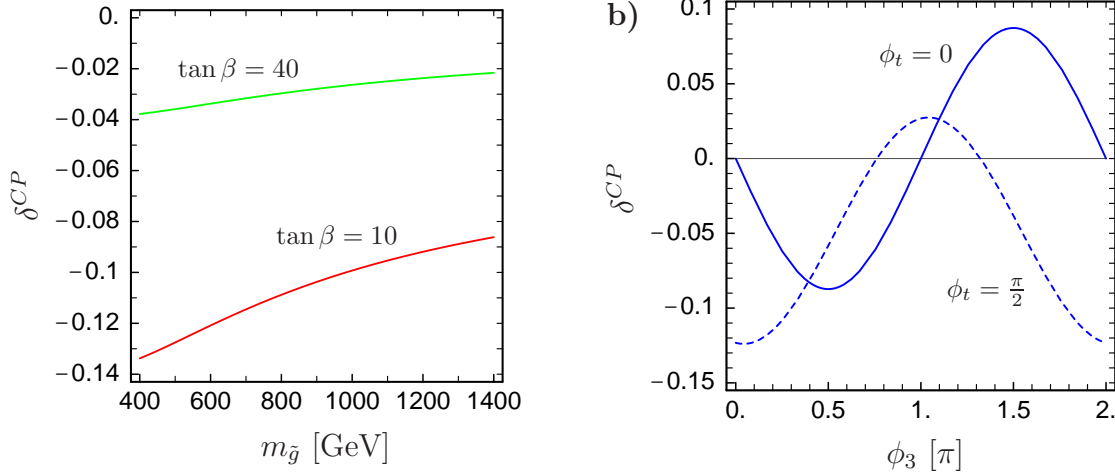


Figure 6: **a)** δ^{CP} as a function of $m_{\tilde{g}}$, for $M_{\tilde{Q}} = 350$ GeV, $m_{H^+} = 700$ GeV, $\phi_t = \pi/2$, and $\tan \beta = 10$ and 40 . **b)** δ^{CP} as a function of ϕ_3 , the phase of M_3 , for $m_{\tilde{g}} = 565$ GeV, $M_{\tilde{Q}} = 350$ GeV, $m_{H^+} = 700$ GeV, $\tan \beta = 10$, $\phi_t = 0$ (full line) and $\phi_t = \pi/2$ (dashed line). $\phi_b = 0$, the other parameters are fixed by Eq. (27).

5 Conclusions

We have calculated the difference between the partial rates $\Gamma(H^+ \rightarrow t\bar{b})$ and $\Gamma(H^- \rightarrow t\bar{b})$ due to CP-violating phases in the MSSM. The resulting decay rate asymmetry δ^{CP} , Eq. (1), could be measured in a counting experiment. If $m_{H^+} < m_{\tilde{t}_1} + m_{\tilde{b}_1}$, δ^{CP} is typically of the order of 10^{-3} . However, for $m_{H^+} > m_{\tilde{t}_1} + m_{\tilde{b}_1}$, δ^{CP} can go up to 10–15%, depending on the phases of A_t and A_b , and on $\tan \beta$. Also a phase of M_3 can have a large effect.

At the Tevatron, no sensitivity for detecting H^\pm is expected for a mass $m_{H^+} \gtrsim 200$ GeV. The LHC, on the other hand, has a discovery reach up to $m_{H^+} \sim 1$ TeV, especially if QCD and SUSY effects conspire to enhance the cross section. With a luminosity of $\mathcal{L} = 100 \text{ fb}^{-1}$, about

217 signal events can be expected for $pp \rightarrow H^+ \bar{t} b$ with $S/\sqrt{B} = 6.3$ (B being the background), for $m_{H^+} \simeq 700$ GeV and $\tan \beta = 50$ [16]. In e^+e^- collisions, the dominant production mode is $e^+e^- \rightarrow H^+H^-$. Therefore, one would need a centre-of-mass energy $\sqrt{s} > 2m_{H^+}$. This would certainly be realized at a multi-TeV linear collider such as CLIC [17]. Hence, a CP-violating asymmetry δ^{CP} of a few per cent should be measurable at the LHC or CLIC.

Acknowledgements

We thank Johann Kühn and Werner Porod for helpful discussions. We also thank Marco Fabbrichesi for his participation in the initial stage of this work. The work of E.C. was supported by the Bulgarian National Science Foundation, Grant Ph-1010.

A Masses and mixing matrices

The **neutralino** mass matrix in the basis of

$$\Psi_j^0 = (-i\lambda', -i\lambda^3, \psi_{H_1}^0, \psi_{H_2}^0) \quad (28)$$

is:

$$\mathcal{M}_N = \begin{pmatrix} M_1 & 0 & -m_Z \sin \theta_W \cos \beta & m_Z \sin \theta_W \sin \beta \\ 0 & M_2 & m_Z \cos \theta_W \cos \beta & -m_Z \cos \theta_W \sin \beta \\ -m_Z \sin \theta_W \cos \beta & m_Z \cos \theta_W \cos \beta & 0 & -\mu \\ m_Z \sin \theta_W \sin \beta & -m_Z \cos \theta_W \sin \beta & -\mu & 0 \end{pmatrix} \quad (29)$$

with $\tan \beta = v_2/v_1$. This matrix is diagonalized by the unitary mixing matrix N :

$$N^* \mathcal{M}_N N^\dagger = \text{diag}(m_{\tilde{\chi}_1^0}, m_{\tilde{\chi}_2^0}, m_{\tilde{\chi}_3^0}, m_{\tilde{\chi}_4^0}), \quad (30)$$

where $m_{\tilde{\chi}_k^0}$, $k = 1, \dots, 4$, are the (non-negative) masses of the physical neutralino states.

The **chargino** mass matrix is:

$$\mathcal{M}_C = \begin{pmatrix} M_2 & \sqrt{2} m_W \sin \beta \\ \sqrt{2} m_W \cos \beta & \mu \end{pmatrix}. \quad (31)$$

It is diagonalized by the two unitary matrices U and V :

$$U^* \mathcal{M}_C V^\dagger = \text{diag}(m_{\tilde{\chi}_1^+}, m_{\tilde{\chi}_2^+}), \quad (32)$$

where $m_{\tilde{\chi}_{1,2}^+}$ are the masses of the physical chargino states.

The mass matrix of the **stops** in the basis $(\tilde{t}_L, \tilde{t}_R)$ is

$$\mathcal{M}_t^2 = \begin{pmatrix} M_{\tilde{Q}}^2 + m_Z^2 \cos 2\beta (\frac{1}{2} - \frac{2}{3} \sin^2 \theta_W) + m_t^2 & (A_t^* - \mu \cot \beta) m_t \\ (A_t - \mu^* \cot \beta) m_t & M_{\tilde{U}}^2 + \frac{2}{3} m_Z^2 \cos 2\beta \sin^2 \theta_W + m_t^2 \end{pmatrix}. \quad (33)$$

\mathcal{M}_t^2 is diagonalized by the rotation matrix $R^{\tilde{t}}$ such that $R^{\tilde{t}\dagger} \mathcal{M}_t^2 R^{\tilde{t}} = \text{diag}(m_{\tilde{t}_1}^2, m_{\tilde{t}_2}^2)$ and $\begin{pmatrix} \tilde{t}_L \\ \tilde{t}_R \end{pmatrix} = R^{\tilde{t}} \begin{pmatrix} \tilde{t}_1 \\ \tilde{t}_2 \end{pmatrix}$. We have:

$$R^{\tilde{t}} = \begin{pmatrix} R_{L1}^{\tilde{t}} & R_{L2}^{\tilde{t}} \\ R_{R1}^{\tilde{t}} & R_{R2}^{\tilde{t}} \end{pmatrix} = \begin{pmatrix} e^{\frac{i}{2}\varphi_{\tilde{t}}} \cos \theta_{\tilde{t}} & -e^{\frac{i}{2}\varphi_{\tilde{t}}} \sin \theta_{\tilde{t}} \\ e^{-\frac{i}{2}\varphi_{\tilde{t}}} \sin \theta_{\tilde{t}} & e^{-\frac{i}{2}\varphi_{\tilde{t}}} \cos \theta_{\tilde{t}} \end{pmatrix}. \quad (34)$$

Analogously, the mass matrix of the **sbottoms** in the basis $(\tilde{b}_L, \tilde{b}_R)$,

$$\mathcal{M}_b^2 = \begin{pmatrix} M_{\tilde{Q}}^2 - m_Z^2 \cos 2\beta (\frac{1}{2} - \frac{1}{3} \sin^2 \theta_W) + m_b^2 & (A_b^* - \mu \tan \beta) m_b \\ (A_b - \mu^* \tan \beta) m_b & M_{\tilde{D}}^2 - \frac{1}{3} m_Z^2 \cos 2\beta \sin^2 \theta_W + m_b^2 \end{pmatrix}, \quad (35)$$

is diagonalized by the rotation matrix $R^{\tilde{b}}$ such that $R^{\tilde{b}\dagger} \mathcal{M}_b^2 R^{\tilde{b}} = \text{diag}(m_{\tilde{b}_1}^2, m_{\tilde{b}_2}^2)$.

In the **neutral Higgs sector**, we have two CP-even states $\phi_i = \sqrt{2} \text{Re}(\mathcal{H}_i^i) - v_i$, $i = 1, 2$, and one CP-odd state $a = \sqrt{2} (-\sin \beta \text{Im}(\mathcal{H}_1^1) + \cos \beta \text{Im}(\mathcal{H}_2^2))$, where \mathcal{H}_1 and \mathcal{H}_2 are the two Higgs doublets in the interaction basis. In the basis (ϕ_1, ϕ_2, a) , the neutral Higgs mass matrix \mathcal{M}_H^2 can be written as the well-known tree-level part, which has a block form in this

basis, plus a general 3×3 matrix containing the loop corrections:

$$\mathcal{M}_H^2 = \begin{pmatrix} s^2\beta m_A^2 + c^2\beta m_Z^2 & -s\beta c\beta (m_A^2 + m_Z^2) & 0 \\ -s\beta c\beta (m_A^2 + m_Z^2) & c^2\beta m_A^2 + s^2\beta m_Z^2 & 0 \\ 0 & 0 & m_A^2 \end{pmatrix} + \left(\mathcal{M}_H^{\text{loop}}\right)^2, \quad (36)$$

where $s\beta \equiv \sin \beta$, $c\beta \equiv \cos \beta$, etc. In the case of complex parameters, the loop contributions of $(\mathcal{M}_H^{\text{loop}})^2$ lead to a mixing of the CP-even and CP-odd states. The mass eigenstates then are

$$\begin{pmatrix} H_1^0 \\ H_2^0 \\ H_3^0 \end{pmatrix} = O^T \cdot \begin{pmatrix} \phi_1 \\ \phi_2 \\ a \end{pmatrix}. \quad (37)$$

The real 3×3 rotation matrix O diagonalizes the mass matrix \mathcal{M}_H^2 ,

$$O^T \mathcal{M}_H^2 O = \text{diag} \left(m_{H_1^0}^2, m_{H_2^0}^2, m_{H_3^0}^2 \right), \quad (38)$$

with $m_{H_1^0} < m_{H_2^0} < m_{H_3^0}$. The transformations of the Higgs fields from the interaction basis to the mass eigenstate basis are given by

$$\begin{aligned} \mathcal{H}_1^1 &= v_1 + \frac{1}{\sqrt{2}} \left[(O_{1j} + i \sin \beta O_{3j}) H_j^0 - i \cos \beta G^0 \right], \\ \mathcal{H}_1^2 &= -\cos \beta G^- + \sin \beta H^-, \\ \mathcal{H}_2^1 &= \sin \beta G^+ + \cos \beta H^+, \\ \mathcal{H}_2^2 &= v_2 + \frac{1}{\sqrt{2}} \left[(O_{2j} + i \cos \beta O_{3j}) H_j^0 + i \sin \beta G^0 \right], \end{aligned} \quad (39)$$

with the implicit sum over $j = 1, 2, 3$,

$$v_1 = v \cos \beta = \frac{\sqrt{2}}{g} m_W \cos \beta, \quad v_2 = v \sin \beta = \frac{\sqrt{2}}{g} m_W \sin \beta. \quad (40)$$

For the numerical evaluation of the physical Higgs masses and the rotation matrix O in the 1-loop effective potential approach [8], we use the program `chp.f` [12].

B Interaction Lagrangian

In this section we give the parts of the interaction Lagrangian that we need for our calculation.

We start with the interaction of Higgs bosons with quarks and squarks:

$$\mathcal{L}_{Hqq} = H^+ \bar{t} (y_b P_R + y_t P_L) b + H^- \bar{b} (y_t P_R + y_b P_L) t + H_l^0 \bar{q} (s_l^{q,R} P_R + s_l^{q,L} P_L) q, \quad (41)$$

$$\mathcal{L}_{H\tilde{q}\tilde{q}} = (G_4)_{ij} H^+ \tilde{t}_i^* \tilde{b}_j + (G_4^*)_{ij} H^- \tilde{b}_j^* \tilde{t}_i, \quad (42)$$

with $i, j = 1, 2, l = 1, 2, 3$ and

$$P_L = \frac{1}{2}(1 - \gamma_5), \quad P_R = \frac{1}{2}(1 + \gamma_5). \quad (43)$$

For the H^\pm couplings to quarks we have

$$y_t = h_t \cos \beta, \quad y_b = h_b \sin \beta, \quad (44)$$

with

$$h_t = \frac{g \overline{m}_t}{\sqrt{2} m_W \sin \beta}, \quad h_b = \frac{g \overline{m}_b}{\sqrt{2} m_W \cos \beta}, \quad (45)$$

where \overline{m}_q is the \overline{DR} running quark mass. For the H_l^0 couplings to quarks we have

$$s_l^{q,R} = -\frac{g \overline{m}_q}{2 m_W} (g_{H_l qq}^S + i g_{H_l qq}^P), \quad (46)$$

$$s_l^{q,L} = -\frac{g \overline{m}_q}{2 m_W} (g_{H_l qq}^S - i g_{H_l qq}^P), \quad (47)$$

with $g_{H_l qq}^S$ and $g_{H_l qq}^P$ given by Eqs. (4.11)–(4.14) in [8]. The H^\pm couplings to squarks are given by the matrix

$$G_4 = R^{\tilde{t}\dagger} \hat{G}_4 R^{\tilde{b}}, \quad (48)$$

with

$$\hat{G}_4 = \begin{pmatrix} h_b m_b \sin \beta + h_t m_t \cos \beta - \sqrt{2} g m_W \sin \beta \cos \beta & h_b (A_b^* \sin \beta + \mu \cos \beta) \\ h_t (A_t \cos \beta + \mu^* \sin \beta) & h_t m_b \cos \beta + h_b m_t \sin \beta \end{pmatrix}. \quad (49)$$

The interactions of charginos and neutralinos are described by

$$\mathcal{L}_{H\tilde{\chi}\tilde{\chi}} = H^+ \tilde{\chi}_i^+ (F_{ik}^R P_R + F_{ik}^L P_L) \tilde{\chi}_k^0 + H^- \tilde{\chi}_k^0 (F_{ik}^{R*} P_L + F_{ik}^{L*} P_R) \tilde{\chi}_i^+, \quad (50)$$

$$\begin{aligned} \mathcal{L}_{q\tilde{q}\tilde{\chi}^+} &= \bar{t} (l_{ij}^{\tilde{b}} P_R + k_{ij}^{\tilde{b}} P_L) \tilde{\chi}_j^+ \tilde{b}_i + \bar{b} (l_{ij}^{\tilde{t}} P_R + k_{ij}^{\tilde{t}} P_L) \tilde{\chi}_j^{+c} \tilde{t}_i \\ &\quad + \overline{\tilde{\chi}_j^+} (l_{ij}^{\tilde{b}*} P_L + k_{ij}^{\tilde{b}*} P_R) t \tilde{b}_i^* + \overline{\tilde{\chi}_j^{+c}} (l_{ij}^{\tilde{t}*} P_L + k_{ij}^{\tilde{t}*} P_R) b \tilde{t}_i^*, \end{aligned} \quad (51)$$

$$\mathcal{L}_{q\tilde{q}\tilde{\chi}^0} = \bar{q} (a_{ik}^{\tilde{q}} P_R + b_{ik}^{\tilde{q}} P_L) \tilde{\chi}_k^0 \tilde{q}_i + \tilde{\chi}_k^0 (a_{ik}^{\tilde{q}*} P_L + b_{ik}^{\tilde{q}*} P_R) q \tilde{q}_i^*, \quad (52)$$

with $i, j = 1, 2$ and $k = 1, \dots, 4$. The couplings of H^\pm to charginos and neutralinos are

$$F_{ik}^R = -g \left[V_{i1} N_{k4} + \frac{1}{\sqrt{2}} (N_{k2} + N_{k1} \tan \theta_W) V_{i2} \right] \cos \beta, \quad (53)$$

$$F_{ik}^L = -g \left[U_{i1}^* N_{k3}^* - \frac{1}{\sqrt{2}} (N_{k2}^* + N_{k1}^* \tan \theta_W) U_{i2}^* \right] \sin \beta. \quad (54)$$

The chargino–squark–quark couplings are

$$l_{ij}^{\tilde{t}} = -g V_{j1} R_{1i}^{\tilde{t}} + h_t V_{j2} R_{2i}^{\tilde{t}}, \quad l_{ij}^{\tilde{b}} = -g U_{j1} R_{1i}^{\tilde{b}} + h_b U_{j2} R_{2i}^{\tilde{b}}, \quad (55)$$

$$k_{ij}^{\tilde{t}} = h_b U_{j2}^* R_{1i}^{\tilde{t}}, \quad k_{ij}^{\tilde{b}} = h_t V_{j2}^* R_{1i}^{\tilde{b}}. \quad (56)$$

The neutralino–squark–quark couplings are

$$a_{ik}^{\tilde{q}} = g f_{Lk}^{\tilde{q}} R_{1i}^{\tilde{q}} + h_{Lk}^{\tilde{q}*} R_{2i}^{\tilde{q}}, \quad (57)$$

$$b_{ik}^{\tilde{q}} = h_{Lk}^{\tilde{q}} R_{1i}^{\tilde{q}} + g f_{Rk}^{\tilde{q}} R_{2i}^{\tilde{q}}, \quad (58)$$

with

$$f_{Lk}^{\tilde{t}} = -\frac{1}{\sqrt{2}} (N_{k2} + \frac{1}{3} \tan \theta_W N_{k1}), \quad f_{Lk}^{\tilde{b}} = \frac{1}{\sqrt{2}} (N_{k2} - \frac{1}{3} \tan \theta_W N_{k1}), \quad (59)$$

$$f_{Rk}^{\tilde{t}} = \frac{2\sqrt{2}}{3} \tan \theta_W N_{k1}^*, \quad f_{Rk}^{\tilde{b}} = -\frac{\sqrt{2}}{3} \tan \theta_W N_{k1}^*, \quad (60)$$

$$h_{Lk}^{\tilde{t}} = -h_t N_{k4}^*, \quad h_{Lk}^{\tilde{b}} = -h_b N_{k3}^*. \quad (61)$$

Finally, the squark–quark–gluino interaction is given by

$$\begin{aligned} \mathcal{L}_{q\tilde{q}\tilde{g}} = & -\sqrt{2} g_s T_{st}^a \left[\tilde{g}^a (R_{1i}^{\tilde{q}} e^{-\frac{i}{2}\phi_3} P_L - R_{2i}^{\tilde{q}} e^{\frac{i}{2}\phi_3} P_R) q_s \tilde{q}_{i,t}^* \right. \\ & \left. + \bar{q}_s (R_{1i}^{\tilde{q}*} e^{\frac{i}{2}\phi_3} P_R - R_{2i}^{\tilde{q}*} e^{-\frac{i}{2}\phi_3} P_L) \tilde{g}^a \tilde{q}_{i,t} \right], \end{aligned} \quad (62)$$

and the quark interaction with W bosons is

$$\mathcal{L}_{qqW} = -\frac{g}{\sqrt{2}} (W_\mu^+ \bar{t} \gamma^\mu P_L b + W_\mu^- \bar{b} \gamma^\mu P_L t). \quad (63)$$

We next turn to the interaction of Higgs bosons with W bosons and ghosts. The Lagrangian of two Higgs particles and one W boson is given by

$$\mathcal{L}_{HHW} = -i \frac{g}{\sqrt{2}} \left[W_\mu^+ \left(\mathcal{H}_1^{1*} \overset{\leftrightarrow}{\partial}^\mu \mathcal{H}_1^2 + \mathcal{H}_2^{1*} \overset{\leftrightarrow}{\partial}^\mu \mathcal{H}_2^2 \right) + W_\mu^- \left(\mathcal{H}_1^1 \overset{\leftrightarrow}{\partial}^\mu \mathcal{H}_1^{2*} + \mathcal{H}_2^1 \overset{\leftrightarrow}{\partial}^\mu \mathcal{H}_2^{2*} \right) \right], \quad (64)$$

where

$$A \overset{\leftrightarrow}{\partial}^\mu B = A (\partial_\mu B) - (\partial_\mu A) B. \quad (65)$$

Using the transformations Eq. (39) we get

$$\mathcal{L}_{HHW} = i \frac{g}{2} \left[W_\mu^+ \left(g_{H_j H^- W^+} H_j^0 \overset{\leftrightarrow}{\partial}^\mu H^- + g_{H_j G^- W^+} H_j^0 \overset{\leftrightarrow}{\partial}^\mu G^- + i G^0 \overset{\leftrightarrow}{\partial}^\mu G^- \right) + \text{h.c.} \right] \quad (66)$$

where

$$g_{H_j H^- W^+} = -\sin \beta O_{1j} + \cos \beta O_{2j} + i O_{3j} \quad \text{and} \quad (67)$$

$$g_{H_j G^- W^+} = \cos \beta O_{1j} + \sin \beta O_{2j}. \quad (68)$$

Moreover, $g_{H_j H^+ W^-} = g_{H_j H^- W^+}^*$ and $g_{H_j G^+ W^-} = g_{H_j G^- W^+}$. Note that there is no $G^0 W^\pm H^\mp$ coupling. We further need the couplings of two charged and one neutral Higgs bosons. They are derived from the D -term interaction Lagrangian of the Higgs sector,

$\mathcal{L} = -\frac{1}{2} (D' D' + D^1 D^1 + D^2 D^2 + D^3 D^3)$, where D' and D^i are the $U(1)_Y$ and $SU(2)_I$ D -terms, respectively. In terms of Higgs fields in the interaction basis we have

$$\begin{aligned} \mathcal{L}_{HHH} = & -\frac{1}{8} (g^2 + g'^2) (\mathcal{H}_1^{1*} \mathcal{H}_1^1 + \mathcal{H}_1^{2*} \mathcal{H}_1^2 - \mathcal{H}_2^{1*} \mathcal{H}_2^1 - \mathcal{H}_2^{2*} \mathcal{H}_2^2) \\ & - \frac{g^2}{2} (\mathcal{H}_1^{1*} \mathcal{H}_2^1 + \mathcal{H}_1^{2*} \mathcal{H}_2^2) (\mathcal{H}_1^1 \mathcal{H}_2^{1*} + \mathcal{H}_1^2 \mathcal{H}_2^{2*}). \end{aligned} \quad (69)$$

The Lagrangian in the mass eigenstate basis is again obtained by applying the transformations of Eqs. (39) and (40). We are only interested in the combinations of $(H_l^0, G^0) \times (H^\pm, G^\pm) \times (H^\mp, G^\mp)$. The couplings to G^0 , e.g. $G^0 H^+ H^-$, $G^0 H^+ G^-$, $G^0 G^+ H^-$, and $G^0 G^+ G^-$, are zero. The couplings to H_l^0 are:

$$\begin{aligned} \mathcal{L}_{HHH} = & g_{H_j H^+ H^-} H_j^0 H^+ H^- + g_{H_j H^+ G^-} H_j^0 H^+ G^- \\ & + g_{H_j H^+ G^-}^* H_j^0 G^+ H^- + g_{H_j G^+ G^-} H_j^0 G^+ G^-, \end{aligned} \quad (70)$$

with

$$g_{H_j H^+ H^-} = \frac{g m_W}{2} \{ [(1 + t_W^2) c 2\beta - 2] c\beta O_{1j} - [(1 + t_W^2) c 2\beta + 2] s\beta O_{2j} \}, \quad (71)$$

$$g_{H_j H^+ G^-} = \frac{g m_W}{2} [c 2\beta (s\beta O_{1j} + c\beta O_{2j}) - i O_{3j} + t_W^2 s 2\beta (c\beta O_{1j} - s\beta O_{2j})], \quad (72)$$

$$g_{H_j G^+ G^-} = -\frac{g m_W}{2} (1 + t_W^2) c 2\beta (c\beta O_{1j} - s\beta O_{2j}). \quad (73)$$

Note that only $g_{H_j H^+ G^-}$ is complex. In Eqs. (71)–(73), we have used the abbreviations $s\beta \equiv \sin \beta$, $s2\beta \equiv \sin 2\beta$, $c\beta \equiv \cos \beta$, $c2\beta \equiv \cos 2\beta$, and $t_W^2 \equiv \tan^2 \theta_W$.

C Passarino–Veltman integrals

Here we give the definition of the Passarino–Veltman one-, two-, and three-point functions [9] in the convention of [10]. For the general denominators we use the notation

$$\mathcal{D}^0 = q^2 - m_0^2 \quad \text{and} \quad \mathcal{D}^j = (q + p_j)^2 - m_j^2. \quad (74)$$

Then the loop integrals in $D = 4 - \epsilon$ dimensions are as follows:

$$A_0(m_0^2) = \frac{1}{i\pi^2} \int d^D q \frac{1}{\mathcal{D}^0}, \quad (75)$$

$$B_0(p_1^2, m_0^2, m_1^2) = \frac{1}{i\pi^2} \int d^D q \frac{1}{\mathcal{D}^0 \mathcal{D}^1}, \quad (76)$$

$$B_\mu(p_1^2, m_0^2, m_1^2) = \frac{1}{i\pi^2} \int d^D q \frac{q_\mu}{\mathcal{D}^0 \mathcal{D}^1} = p_{1\mu} B_1(p_1^2, m_0^2, m_1^2), \quad (77)$$

and

$$C_0 = \frac{1}{i\pi^2} \int d^D q \frac{1}{\mathcal{D}^0 \mathcal{D}^1 \mathcal{D}^2}, \quad (78)$$

$$C_\mu = \frac{1}{i\pi^2} \int d^D q \frac{q_\mu}{\mathcal{D}^0 \mathcal{D}^1 \mathcal{D}^2} = p_{1\mu} C_1 + p_{2\mu} C_2, \quad (79)$$

$$\begin{aligned} C_{\mu\nu} &= \frac{1}{i\pi^2} \int d^D q \frac{q_\mu q_\nu}{\mathcal{D}^0 \mathcal{D}^1 \mathcal{D}^2} \\ &= g_{\mu\nu} C_{00} + p_{1\mu} p_{1\nu} C_{11} + (p_{1\mu} p_{2\nu} + p_{2\mu} p_{1\nu}) C_{12} + p_{2\mu} p_{2\nu} C_{22}, \end{aligned} \quad (80)$$

where the C 's have $(p_1^2, (p_1 - p_2)^2, p_2^2, m_0^2, m_1^2, m_2^2)$ as their arguments. The function B_1 can be expressed as a combination of the functions A_0 and B_0 :

$$2p_1^2 B_1(p_1^2, m_0^2, m_1^2) = A_0(m_0^2) - A_0(m_1^2) - (p_1^2 - m_1^2 + m_0^2) B_0(p_1^2, m_0^2, m_1^2). \quad (81)$$

References

- [1] M. Dugan, B. Grinstein and L. J. Hall, Nucl. Phys. B **255** (1985) 413.

- [2] M. Carena, M. Quiros and C. E. Wagner, Nucl. Phys. B **524** (1998) 3 [hep-ph/9710401]; for a review see: A. G. Cohen, D. B. Kaplan and A. E. Nelson, Ann. Rev. Nucl. Part. Sci. **43** (1993) 27 [hep-ph/9302210].
- [3] I. S. Altarev *et al.*, Phys. Lett. B **276** (1992) 242; I. S. Altarev *et al.*, Phys. Atom. Nucl. **59** (1996) 1152 [Yad. Fiz. **59N7** (1996) 1204]; E. D. Commins, S. B. Ross, D. DeMille and B. C. Regan, Phys. Rev. A **50** (1994) 2960.
- [4] P. Nath, Phys. Rev. Lett. **66** (1991) 2565; Y. Kizukuri and N. Oshimo, Phys. Rev. D **46** (1992) 3025; R. Garisto and J. D. Wells, Phys. Rev. D **55** (1997) 1611 [hep-ph/9609511]; Y. Grossman, Y. Nir and R. Rattazzi, Adv. Ser. Direct. High Energy Phys. **15** (1998) 755 [hep-ph/9701231].
- [5] T. Ibrahim and P. Nath, Phys. Lett. B **418** (1998) 98 [hep-ph/9707409]; M. Brhlik, G. J. Good and G. L. Kane, Phys. Rev. D **59** (1999) 115004 [hep-ph/9810457]; A. Bartl, T. Gajdosik, W. Porod, P. Stockinger and H. Stremnitzer, Phys. Rev. D **60** (1999) 073003 [hep-ph/9903402].
- [6] For a review, see: D. Atwood, S. Bar-Shalom, G. Eilam and A. Soni, Phys. Rept. **347** (2001) 1 [hep-ph/0006032].
- [7] A. Pilaftsis, Phys. Rev. D **58** (1998) 096010 [hep-ph/9803297] and Phys. Lett. B **435** (1998) 88 [hep-ph/9805373]; A. Pilaftsis and C. E. Wagner, Nucl. Phys. B **553** (1999) 3 [hep-ph/9902371]; D. A. Demir, Phys. Rev. D **60** (1999) 055006 [hep-ph/9901389].
- [8] M. Carena, J. R. Ellis, A. Pilaftsis and C. E. Wagner, Nucl. Phys. B **586** (2000) 92 [hep-ph/0003180].
- [9] G. Passarino and M. J. Veltman, Nucl. Phys. B **160** (1979) 151.
- [10] A. Denner, Fortschr. Phys. **41** (1993) 307.
- [11] B. C. Allanach *et al.*, hep-ph/0202233, in *Proc. of the APS/DPF/DPB Summer Study on the Future of Particle Physics (Snowmass 2001)*, eds. R. Davidson and C. Quigg.

- [12] The Fortran program `cph.f` can be obtained from
<http://pilaftsi.home.cern.ch/pilaftsi/>
- [13] E. Christova, H. Eberl, S. Kraml and W. Majerotto, Nucl. Phys. B **639** (2002) 263.
- [14] E. Christova, H. Eberl, S. Kraml and W. Majerotto, Erratum to Nucl. Phys. B **639** (2002) 263, to appear.
- [15] M. Carena, J. R. Ellis, A. Pilaftsis and C. E. Wagner, Nucl. Phys. B **625** (2002) 345 [hep-ph/0111245]; S. Heinemeyer, Eur. Phys. J. C **22** (2001) 521 [hep-ph/0108059]; T. Ibrahim and P. Nath, hep-ph/0204092.
- [16] A. Belyaev, D. Garcia, J. Guasch and J. Sola, hep-ph/0203031.
- [17] M. Battaglia, A. Ferrari, A. Kiiskinen and T. Maki, hep-ex/0112015, in *Proc. of the APS/DPF/DPB Summer Study on the Future of Particle Physics (Snowmass 2001)*, eds. R. Davidson and C. Quigg.